Unravelling the Behavior of Dion–Jacobson Layered Hybrid Perovskites in Humid Environments

Algirdas Dučinskas[1,2], Gee Yeong Kim[2], Davide Moia[2], Alessandro Senocrate[2], Ya-Ru Wang[2], Michael A. Hope[3], Aditya Mishra[3], Dominik J. Kubicki[4], Miłosz Siczek[5], Wojciech Bury[5], Thomas Schneeberger[1], Lyndon Emsley[3], Jovana V. Milić[1], Joachim Maier[2*], Michael Grätzel[1*]*

[1] Laboratory of Photonics and Interfaces, EPFL, 1015 Lausanne, Switzerland

[2] Max Planck Institute for Solid State Research, Heisenbergstr. 1, 70569 Stuttgart, Germany

[3] Laboratory of Magnetic Resonance, EPFL, 1015 Lausanne, Switzerland

[4] Cavendish Laboratory, University of Cambridge, CB3 0HE, Cambridge, UK

[5] Faculty of Chemistry, University of Wrocław, F. Joliot-Curie 14, 50-383 Wrocław, Poland

Email: jovana.milic@epfl.ch, jmaier@fkf.mpg.de, michael.graetzel@epfl.ch

ABSTRACT. Layered hybrid halide perovskites have been proven to be more environmentally stable than their 3D analogues. The enhanced stability is particularly relevant for Dion–Jacobson-type layered perovskites due to their promising photovoltaic performances. However, in contrast to the expected resilience to moisture, we reveal that the structure of Dion–Jacobson perovskite phases based on a 1,4–phenylenedimethanamonium spacer is disrupted in humid conditions using X-ray diffraction, UV-vis spectroscopy, thermogravimetric analysis and solid-state NMR

spectroscopy. The process takes place at ≥65 ± 5% relative humidity, with a timescale on the order of minutes. The original layered structure can be restored upon annealing at 150 °C and the hydration can be suppressed by post-synthetic annealing in air, which is attributed to the generation of a self-protective layer of PbI_2. This study thereby reveals a unique behavior of layered perovskites in humid environments, which is critical to their stabilizing role in hybrid perovskite devices.

TOC GRAPHICS

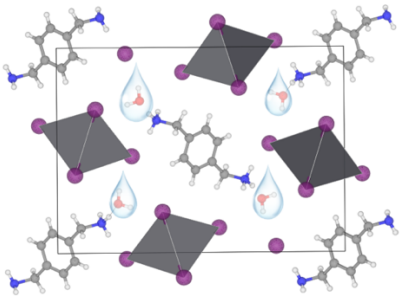

Hybrid halide perovskites have attracted considerable interest in optoelectroncs.[1,2] They have the general formula AMX_3, where A is a monovalent cation (formamidinium (FA^+), methylammonium (MA^+), Cs^+), M a divalent metal (Pb^{2+}, Sn^{2+}) and X a halogen anion (I^-, Br^-, Cl^-). Despite their exceptional photo-electrochemical properties, these materials show poor intrinsic and extrinsic stability (towards temperature, electrical bias, light, oxygen and moisture).[3] A possible strategy to improve stability is to introduce large organic cations which, according to the Goldschmidt tolerance factor, cannot fit into the A site[4], but are able to act as spacer molecules connecting neighboring inorganic layers. The resulting materials are referred to as layered (2D) hybrid perovskites.[5-7] They can be further divided into two main categories, namely Ruddlesden-Popper (RP) phases,[8,9] with chemical formula $A'_2A_{n-1}B_nX_{3n+1}$ based on monovalent organic spacer (A') bilayers, and Dion–Jacobson (DJ) phases defined by the $A''A_{n-1}B_nX_{3n+1}$ formula featuring divalent

spacer (A") monolayers.[10] For both classes of materials, *n* is the number of perovskite layers between each layer of spacer molecules.[11-13] The spacer molecules render 2D hybrid perovskites more resilient to moisture as compared to their 3D counterparts,[14,15] therefore increasing the organic spacer content (i.e. reducing the number of perovskite layers, *n*) is expected to enhance the stability against moisture. Accordingly, it was reported that RP-type layered perovskites based on 2-phenylethylammonium (PEA^+) spacer moieties in $n = 5$ compositions disproportionate upon exposure to humid atmosphere into lower ($n < 5$) compositions.[16] Similar observations apply to butylammonium (BA^+)-based layered hybrid perovskites.[17-19] Moreover, RP perovskites based on a 1-propylamine spacer exhibit inferior stability as compared to DJ perovskites based on 1,3-diaminopropane analogues, which was attributed to the removal of the van der Waals gap present in RP hybrid perovskites.[20] This suggests that the structure of layered perovskites plays an important role in their stability against humidity and that DJ perovskites have the potential to exhibit enhanced moisture tolerance. However, their behavior in humid environments has not been critically assessed. Since bifunctional spacers directly connect the perovskite layers of the DJ phase,[10,21] the reduced layer spacing can improve charge transfer.[22] For this reason, DJ perovskites have been implemented in PV devices and reached a power conversion efficiency of 18%.[23] Even though DJ phases are expected to exhibit improved extrinsic stability, a few hydrated structures have been reported for perovskites based on bifunctional spacers, such as 2-(aminomethylpyridinium)[24] and 1,4-phenylenediammonium.[25] The bifunctionality of the spacer is, however, not the only requirement for the formation of DJ phases and the geometry of the spacer as well as the adaptability of the ammonium groups play an important role.[11,21] For instance, 1,4-phenylenediammonium moieties do not form DJ phases.[25] The examples of hydrated phases

comprising bifunctional spacers suggest that DJ perovskite phases might be prone to hydration, which has so far not been demonstrated, despite its relevance for their optoelectronic applications.

Here, we report a hydration effect in DJ layered hybrid perovskites based on 1,4-phenylenedimethanammonium ($PDMA^{2+}$) spacer, which has been reported to be a promising candidate for PV applications.[11,26,27] In contrast to the expected resilience to moisture, we reveal that thin films and powders of (PDMA)PbI_4 ($n = 1$) undergo hydration upon exposure to $\geq 65 \pm 5\%$ relative humidity, as demonstrated by X-ray diffraction (XRD) and UV-vis absorption spectroscopy, as well as thermogravimetric analysis (TGA) and solid-state NMR spectroscopy. However, the corresponding changes in structural and optical properties could be reverted upon annealing at 150 °C and suppressed by post-synthetic annealing in air. The latter phenomenon was attributed to the generation of PbI_2 that acts as a self-protective layer, retarding humidity-induced changes. This study provides new insights into the behavior of DJ layered hybrid perovskites in humid environments, which is relevant for their application in optoelectronic devices.

Perovskite thin films of (PDMA)PbI_4 were fabricated via spin-coating with a solution obtained by mixing stoichiometric quantities of the corresponding precursors, followed by annealing at 150 °C for 10 min (experimental details are provided in Section S1 of the Supporting information, SI, along with supplementary spectral data, Figures S1–S16). While $n = 1$ compositional representatives, such as (PDMA)PbI_4, might not be the best candidates for photovoltaic applications,[10] they feature the highest content of the spacer layer that are thus expected to present the greatest resilience to moisture. Furthermore, unlike $n > 1$ compositions that form mixtures of quasi-2D and 2D/3D phases in thin films,[5-7] rendering their critical assessment more complex, $n = 1$ compositions are known to form well-defined 2D phases in thin films. Therefore, they

represent appropriate model systems to evaluate the behavior of this class of materials in humid environments.

To confirm the formation of the layered (PDMA)PbI_4 perovskite structure, the films were analyzed by XRD. The diffraction pattern (Figure 1b) exhibits a peak at low diffraction angle (2θ = 7.2°), corresponding to an inter-planar d-spacing of 12.2 Å, which provides a fingerprint of the layered structure.[11, 28] Considering that the $PDMA^{2+}$ molecule length and the $[PbI_6]^{4-}$ octahedron size are both approximately 6 Å (Figure 1a), this peak is attributed to the (001) reflection. The higher order (00*l*) diffraction peaks are found at 14.3, 21.5, and 28.8°. This indicates the presence of crystallites that consist of perovskite layers that are parallel to the substrate.[29,30] The further peak at 14.5° is assigned to the (100) reflection since the corresponding d-spacing of approximately 6 Å is comparable to the size of the $[PbI_6]^{4-}$ octahedron. The (200) reflection is also observed at 29.1° and these correspond to crystallites with the perovskite layers perpendicular to the substrate.[14,31] Thus, crystallites in the analyzed (PDMA)PbI_4 thin films have both perpendicular and parallel orientations, which is in good agreement with previous reports.[11,28,32]

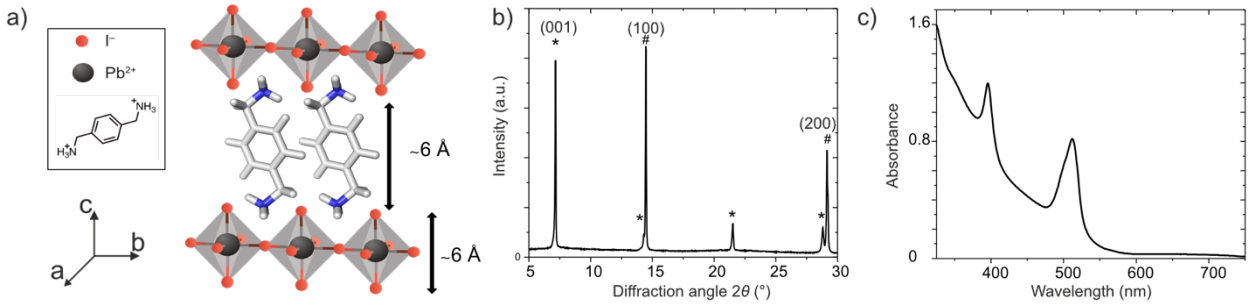

Figure 1. (a) Structural representation of the (PDMA)PbI_4 layered structure. Pb^{2+} is shown in grey, I^- is depicted in dark purple, and the $PDMA^{2+}$ is depicted with its DFT-calculated structure.[37] (b) XRD of (PDMA)PbI_4 thin films on microscope glass. Peaks denoted with * belong to (00*l*) Bragg planes and # to (*h00*) planes. (c) UV-vis spectrum of (PDMA)PbI_4 thin films on microscope glass.

Having demonstrated that (PDMA)PbI_4 forms a layered structure and taking into account that the van der Waals radius of iodide is smaller than the spacing between the inorganic layers,[33] quantum confinement is expected to take place, where the 2D layer of corner-sharing $[PbI_6]^{-4}$ octahedra forms a quantum well structure.[32] Indeed, the UV-vis absorption spectrum of (PDMA)PbI_4 shows a strong excitonic absorption peak located at 510 nm (Figure 1c), which indicates significant confinement of the excitons (exciton binding energy >> kT).[34] In addition to the main excitonic peak, an absorption peak is detected at 395 nm, which could correspond to optical transitions to the Rydberg states.[34] This, however, appears unlikely since the energy difference between the two absorption peaks is 0.7 eV, which is higher than the reported exciton binding energies.[34,35]. Alternatively, the absorption peak could be caused by a secondary phase, which however is not observed by XRD. Amorphous phases such as reaction intermediates incorporating solvent molecules[36] could be responsible for this second feature, however a clear solvent dependence of the absorption peak has not been observed (Figure S10).

Upon exposing the (PDMA)PbI_4 films to 65 ± 5% RH, their color changes and the films become pale (Figure 2a inset). These treated films will be further referred to as *hydrated*. Their UV-Vis absorption spectra (Figure 2a) clearly indicate that the excitonic peak at 510 nm, which is attributed to the layered structure, is suppressed, whereas the 395 nm absorption peak is enhanced. This observation supports the argument that the 395 nm peak is not caused by the optical transitions to a Rydberg state associated with the low energy absorption peak. Such a strong, localized optical absorption at 395 nm suggests that this peak could come from a phase with reduced dimensionality that forms upon hydration, as reported previously for low-dimensional perovskite materials.[38,39] For instance, hydration studies on $MAPbI_3$ revealed that, upon exposure to humid air, $MAPbI_3$ transforms into a 1D hydrated phase,[38,39] which features a localized absorption at c.a. 400 nm, or

to a 0D structure.[38] Earlier studies on 1D iodoplumbates also show optical absorption in the 400 nm region.[40] In addition to the reduction in dimensionality, changes in connectivity between $[PbI_6]^{4-}$ octahedra may cause variation in the optical band gap;[41] 1D perovskites with face-sharing octahedra have larger band gaps than their 2D corner-sharing counterparts.[41] In that regard, the spacing between inorganic perovskite layers may also have an effect on the absorption properties,[42] yet XRD patterns of pristine samples (Figure 1b) do not include signals that reveal larger d-spacings. From this we conclude that the absorption at 395 nm corresponds to a low-dimensional phase, the origin of which is not determined in the pristine sample.

To assess variations in the crystal structure and changes in crystallinity, the structural properties of hydrated (PDMA)PbI_4 samples were analyzed by XRD (Figure 2b, blue). The most intense peaks of hydrated samples are recorded at 8 and 13° without a set of clear (00*l*) reflections, which implies that the layered structure is disrupted. This observation is in agreement with the decrease in the absorption of the excitonic peak. Moreover, the absence of the peak at 12.8° suggests that the samples do not undergo degradation to form PbI_2, unlike 3D halide perovskites under comparable experimental conditions.[38] Furthermore, crystallization from a water-based solution enabled a single crystal to be isolated (experimental details are provided in Section S2 of the SI). The structure determined by XRD (Figure 2b, red, and Figures S1–S4) confirms the propensity to form 1D perovskite-like structures with $PDMA^{2+}$ in the presence of water (crystallographic information is presented in Section S2 and Table S1 of the SI). The crystals were found to have a stoichiometry of (PDMA)$Pb_2I_6 \cdot 2H_2O$, crystallizing in the monoclinic $P2_1/n$ space group, with the $[Pb_2I_6]^{2-}{}_n$ forming an infinite polymeric chain structure along the crystallographic *a*-axis (Figures S1–S2, SI). The $PDMA^{2+}$ cations are also aligned, forming stacks along the same axis, whereby the aromatic rings of neighboring spacers interact by parallel-displaced π···π stacking interactions

with a distance of 3.54 Å. Water molecules and NH_3^+ moieties of the $PDMA^{2+}$ ions are involved in the formation of N-H···O hydrogen bonds, forming ladder-like polymeric chains along the *a*-axis which separate $[Pb_2I_6]^{2-}_n$ polyanions. The simulated XRD pattern of the $(PDMA)Pb_2I_6{\cdot}2H_2O$ structure (Figure 2b, red) closely matches the experimental XRD pattern of the hydrated films (Figure 2b, blue), which indicates that this is the 1D phase that forms on exposure of $(PDMA)PbI_4$ to humidity.

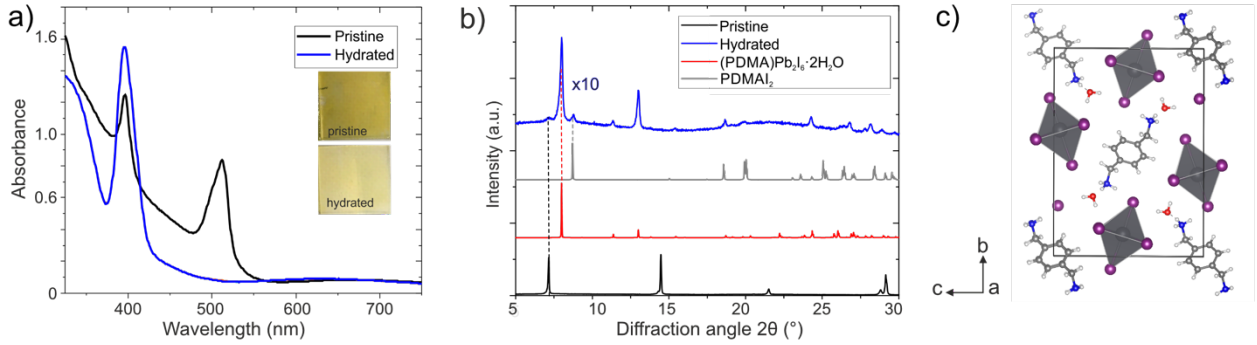

Figure 2. (a) UV-Vis absorption spectra of $(PDMA)PbI_4$ films, before (black) and after (blue) exposure to 65 ± 5% RH. After hydration, the peak at 510 nm is suppressed whereas the one at 395 nm is enhanced. The inset shows photos of pristine (stored in 5 % RH) and hydrated films. (b) XRD patterns of pristine (black), hydrated (blue) films, and the simulated patterns of the hydrated 1D $(PDMA)Pb_2I_6{\cdot}2H_2O$ structure (red; shown in c) and Figure S1–S4) and $(PDMA)I_2$ structure (grey; Figure S5) based on the single crystal analysis, indicating the disruption of the layered structure upon hydration. The XRD intensity of the hydrated sample is multiplied by 10.

However, since the PDMA:Pb ratio is different between the initial 2D DJ and hydrated 1D phases, the hydration reaction must also form $(PDMA)I_2$, according to the following reaction (1).

$$2(PDMA)PbI_4 + 2H_2O \rightarrow (PDMA)Pb_2I_6{\cdot}2H_2O + (PDMA)I_2 \quad (1)$$

This is consistent with the $(PDMA)I_2$ signals observed in the XRD pattern (Figure 2b, grey). The scattering power of the lighter $(PDMA)I_2$ is significantly less than for $(PDMA)Pb_2I_6{\cdot}2H_2O$, but the ratios of the observed reflections are approximately consistent with the expected 1:1 atomic ratio.

In order to quantitatively determine the water uptake by the thin films and powders, we performed thermogravimetric analysis (TGA) on $(PDMA)PbI_4$ powders (Section S3 in the SI). This study reveals that at 35 ± 2% RH there is around 4 at% hydration (Figure S6). In comparison, for the $(PDMA)I_2$ precursor salt, even less hydration was observed (1.8 at% hydration at 35 ± 2% RH, Figure S7). It is assumed that PbI_2 does not hydrate at 35 ± 2% RH, since PbI_2 films do not exhibit changes in optical absorption after exposure to a 65 ± 5% RH atmosphere (Figure S11). This suggests that it is the structure and packing of such layered perovskites that are required for significant hydration, and not the properties of the constituents.[43] The $(PDMA)PbI_4$ powders show a higher water uptake under 65 ± 5% RH conditions; TGA measurements indicate a hydration stoichiometry of 0.98 ± 0.02 H_2O per $PDMA^{2+}$ (Figure S8), in accordance with the 1:1 ratio predicted by reaction (1). Unlike hydrates of $MAPbI_3$ perovskite, which are reported to spontaneously revert back to the initial perovskite structure when returned to a 35% RH atmosphere at room temperature,[38] the hydrated $(PDMA)PbI_4$ phase does not spontaneously convert back to the layered perovskite structure when the humidity is lowered. Dehydration was not observed even when samples were stored under a ~15% RH argon atmosphere (Figure S12). This suggests that the hydrated phase is stable at room temperature.

The structural changes and degree of hydration were further characterized by solid-state NMR of the $(PDMA)I_2$ precursor, mechanosynthesized $(PDMA)PbI_4$ and scraped thin films of hydrated $(PDMA)PbI_4$ (Section S4 in the SI). Following mechanosynthesis of $(PDMA)PbI_4$, significant changes in the ^1H resonances of the $PDMA^{2+}$ moiety are observed compared to the precursor

(PDMA)I_2 salt (Figure S9), corresponding to the substantial change in structure. Upon hydration, the ^{1}H spectrum changes significantly (Figure S9), confirming the considerable structural change shown by XRD. The components arising from (PDMA)$Pb_2I_6 \cdot 2H_2O$ and (PDMA)I_2 cannot be fully resolved, however and additional intensity corresponding to the H_2O is observed and quantification of the ^{1}H spectrum yields a hydration stoichiometry of 0.86 – 0.99 H_2O per $PDMA^{2+}$ (Table S2), which shows that the reactivity of the thin films is the same as for the powders studied by TGA.

To probe the reversibility of the hydration process, in-situ temperature dependent XRD measurements were performed starting from already hydrated powders. Upon heating under nitrogen atmosphere, the hydrated form reverts back to the layered structure at 150 °C, as shown by the disappearance of the diffraction peaks at 8, 9 and 13° (Figure S13). Comparable diffraction patterns are observed for pristine and dehydrated samples (Figure 3d), however the crystallinity of the dehydrated (PDMA)PbI_4 is lower compared to the pristine sample. Furthermore, no signals of PbI_2 species can be distinguished, which excludes irreversible degradation during the hydration–dehydration process. In addition, upon dehydration (150 °C for 10 min under inert atmosphere), the absorption spectra of dehydrated (PDMA)PbI_4 films closely resemble those of the pristine films (Figure 3a). The recovery of the optical properties was further assessed by measuring photoluminescence (PL) (Figure 3b). While pristine films emit at 517 nm, hydrated samples have broad and weak emission in the range of 400–470 nm. This PL signal is expected to originate from the hydrated phase via trap-assisted emission.[44] Dehydrated samples exhibit strong emission at 518 nm accompanied by a broad emission in the range of 400–470 nm. These results suggest a partial reversibility of the hydration-induced structural and optoelectronic changes.

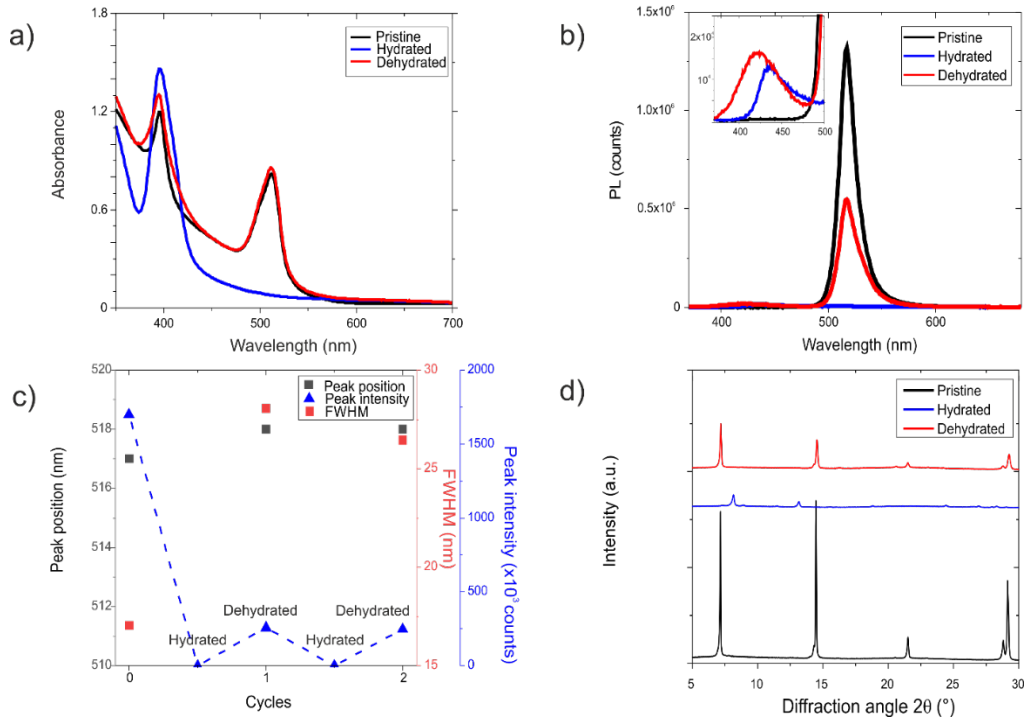

Figure 3. (a) UV-Vis absorption spectra of (PDMA)PbI_4 films at different states of hydration. (b) PL emission spectra; the inset shows emission in the region of 370 nm to 500 nm, which is attributed to the hydrated (lower dimensional) phase. Dehydrated samples were heated at 150 °C for 10 min under argon. (c) Evolution of PL parameters: peak position (black rectangles), full width at half maximum (FWHM) (red rectangles) and PL peak intensity (blue triangles) over two hydration and dehydration cycles. (d) XRD diffraction patterns of pristine (black), hydrated (blue) and dehydrated (red) films also indicate reversible nature of the process.

In order to further address the reversibility of this process, PL emission properties were monitored for two consecutive hydration–dehydration cycles (Figure 3c). Pristine films exhibit stronger and narrower PL emission than films after hydration–dehydration, however the PL emission properties of films after the first and second hydration–dehydration cycles are closely comparable. The drop in PL intensity and peak broadening could be attributed to the structural rearrangements during the 1st hydration-dehydration cycle and reduced sample crystallinity

(Figure 3d). Such changes in structural and optoelectronic properties upon hydration are observed for the thin films of (PDMA)$FAPb_2I_7$ n = 2 composition as well, indicating that higher compositional representatives are also prone to hydration under comparable mechanism (Figure S14). However, unlike n = 1 compositions, they show a lower level of reversibility under comparable experimental conditions, which is likely to be associated with higher structural rearrangements that require further analysis which is beyond the scope of this investigation.

The reversibility of water-induced changes of structural and optoelectronic properties is highly relevant to the protective role of 2D perovskites in perovskite solar cells. For this purpose, it is important to estimate the rate of such changes. We therefore performed in-situ UV–vis absorption measurements of n = 1 samples exposed to humid (65 ± 5% RH) atmosphere (Figure 4a–c). To determine the kinetic profile of the hydration process, we monitored the evolution of the optical absorption over time (Figure 4a) and analyzed the normalized intensity of optical absorption at 510 nm at different time instances (Figure 4c). The evolution of the absorption suggests that pristine (PDMA)PbI_4 films hydrate within minutes at 65 ± 5% RH. The hydration kinetics are dependent on the relative humidity level, which is in agreement with previous observations,[45,46] with higher RH (~80%) atmospheres causing a faster hydration process (Figure S15).

Thus far, we have analyzed data referring to thin films or powders of (PDMA)PbI_4 which were annealed in argon atmosphere. We now explore the effect of a supplementary post-synthetic annealing (hereinafter referred to as *post-annealing*) step performed either in argon or ambient atmosphere. The hydration is suppressed by post-annealing samples in air at 150 °C for 10 min prior to the hydration step, with the samples showing a remarkably improved resilience to moisture (Figure 4b). Comparison of the optical absorption as a function of time (Figure 4c) unambiguously

shows that the hydration rate is slowed significantly when the sample had been post-annealed in air (red curve) as compared to the pristine sample (black curve) or to a sample that had been post-annealed in argon (blue curve).

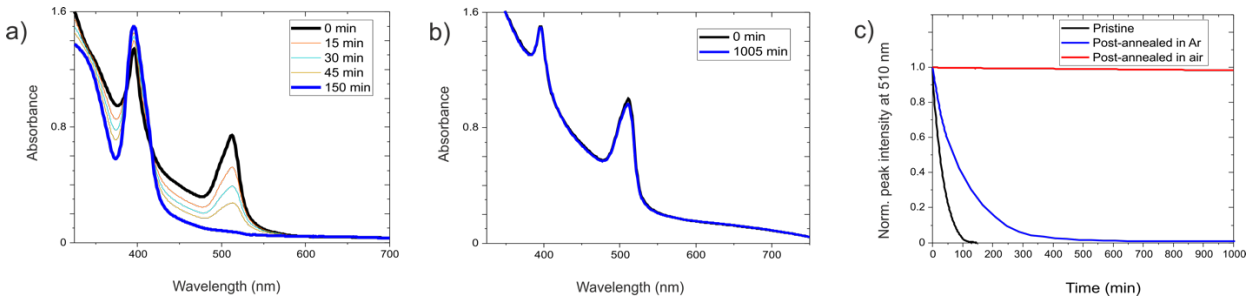

Figure 4. (a) In-situ UV-Vis absorption spectra of pristine (PDMA)PbI_4 films that have been exposed to the 65 ± 5% RH in argon atmosphere for 150 min; the excitonic peak at 510 nm is gradually suppressed and it completely diminishes after 150 min (blue line). (b) In-situ UV-Vis absorption spectra of samples post-annealed in air for 10 min at 150 °C before (black line) and after being exposed to 65 ± 5 % RH argon atmosphere for 16 h and 45 min (blue line). (c) The hydration kinetic profiles of pristine (black), post-annealed in argon (blue) and post-annealed in air (red) samples acquired by monitoring the intensity of the absorption peak at 510 nm. The sample is completely hydrated within 150 min and the sample post-annealed in argon in 500 min, whereas the sample post-annealed in air retains the excitonic peak at 510 nm for at least 1005 min.

To identify the origin of hydration resilience, we performed X-ray photoelectron spectroscopy (XPS) and monitored the changes in surface chemistry. During the post-annealing process in air, (PDMA)PbI_4 may react with oxygen and form PbO/PbO_2;[47] we therefore investigated the possibility of forming such a capping layer that could slow down the hydration. However, Pb 4*f* core level spectra (Figure 5a) show no difference between pristine and post-annealed in air samples, which is corroborated by the I 3d and O 1s spectra (Figure S16), implying that PbO/PbO_2

is not generated upon post-annealing in air. Alternatively, instead of lead oxides, a PbI_2 layer could form during the post-annealing step.[47] This could also act as a protective layer since PbI_2 films do not appear to hydrate upon exposure to humidity, as monitored by in-situ UV-Vis measurements (Figure S11). As the chemical environments of Pb^{2+} ions in (PDMA)PbI_4 and PbI_2 are comparable, XPS is unable to discern the difference. Therefore, we analyzed the films using grazing-incidence XRD measurements. The recorded diffraction patterns of pristine samples and those post-annealed in argon and air (Figure 5b) do not exhibit significant differences in either peak positions or peak intensities, in accordance with a comparable crystal structure for all samples. However, the inset shows that post-annealed in air samples feature a very small diffraction peak at 12.8°, which corresponds to PbI_2. After longer post-annealing in air the diffraction peak at 12.8° becomes more pronounced (Figure S17) strongly indicating that during this process the PbI_2 is gradually generated.

Based on the observation of low degree of hydration for PbI_2 thin films (Figure S11), this result suggests that PbI_2 formation may be responsible for the increased resilience to hydration of samples post-annealed in air. Another possibility is that the difference in hydration rates is due to differences in the sample microstructure. For example, assuming that water molecules have a faster diffusion through grain boundaries, the hydration of polycrystalline materials with larger grains should be slower. Atomic force microscopy (AFM) images of pristine (PDMA)PbI_4 films reveal large grains of several μm (Figure 5c). Upon post-annealing in air, the sample roughness increases, yet the grain size remains comparable (Figure 5d). We can thus conclude that the morphology does not significantly contribute to the suppression of the hydration, which can instead be mainly attributed to the generation of PbI_2. However, future work will be needed to assess if and how the grain boundaries are involved in the hydration process, as well as to determine a detailed

mechanistic understanding of this phenomenon. From our findings, we infer that during the post-annealing process in air, a thin ~~capping~~ self-protective layer of PbI_2 is generated and that consequently the structure and optical absorption of post-annealed 2D perovskites stabilize in humid environments. This provides a new route for increasing the moisture stability of layered hybrid perovskites. Furthermore, the analysis of the 2D $n = 1$ composition provides the basis for extending the understanding to $n > 1$ quasi-2D and 2D/3D perovskite systems that are expected to be highly relevant for photovoltaic applications in the future.

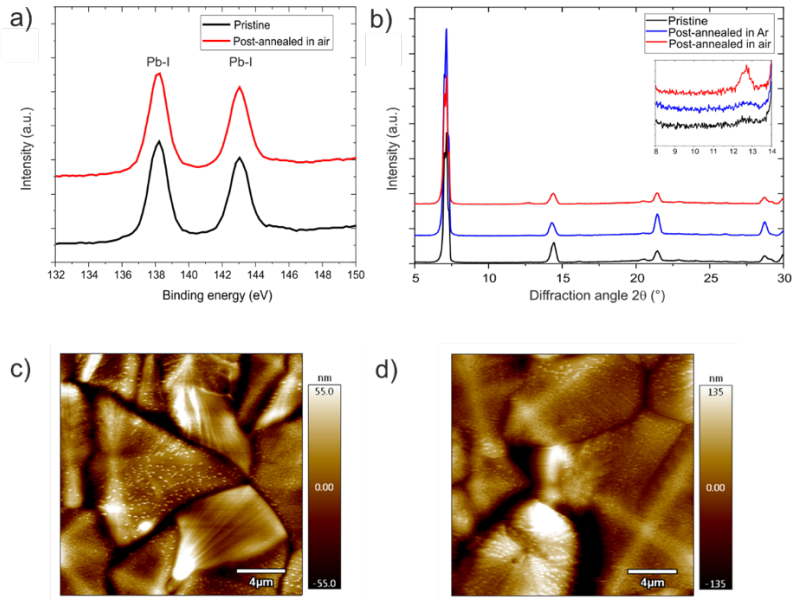

Figure 5. (a) X-ray photoelectron spectra (XPS) in the Pb 4*f* core level range of pristine (black) and post-annealed (red) samples of (PDMA)PbI_4. (b) Grazing incidence XRD measurements of pristine (black), post-annealed in argon (blue) and post-annealed in air (red) samples of (PDMA)PbI_4 before hydration indicate comparable crystal structures. However, the inset shows a very small PbI_2 peak that is apparent when the sample is post-annealed in air. (c–d) Surface morphology images obtained by atomic force microscopy (AFM) suggest that both pristine (c) and post-annealed (d) films consist of grains that are of comparable size. Post-annealing was performed for 10 min at 150 °C in air.

In conclusion, we have investigated the effect of humidity on Dion–Jacobson-type 2D layered hybrid perovskites of (PDMA)PbI_4 composition. Within minutes of exposure to 65 ± 5% RH, a structural transformation takes place that disrupts the layered perovskite structure, as observed by XRD, solid-state NMR and UV-vis optical absorption spectroscopy. The formation of 1D perovskite-like chains with water molecules is further evidenced by single crystal X-ray structure analysis. The observed hydration-induced processes are partially reversible when annealing the powders and thin films at 150 °C in inert atmosphere, while the rate of hydration could be retarded by post-synthetic annealing in air before exposure to humidity. We assign this effect to the formation of a thin layer of PbI_2, which likely protects the 2D perovskite. This study thereby evidences the tendency of a 2D DJ layered perovskite to hydrate in humid atmosphere. Moreover, it provides a new strategy to improve the resilience of layered hybrid perovskites against moisture, which is relevant for the stabilization of hybrid perovskite-based optoelectronic devices.

ASSOCIATED CONTENT

Materials and methods, X-ray crystal structure analysis, TGA data for (PDMA)PbI_4 and (PDMA)I_2 powders, solid-state NMR spectroscopy data, and supplementary spectral data are available as part of the Supplementary Information.

AUTHOR INFORMATION

@lpi_epfl, @epfl_en, @mpifkf, @WCh_UWr, @ducinskas, @jovana_v_milic, @lyndon_emsley, @michael_a_hope, @WojBur

ACKNOWLEDGMENT

Authors are grateful to the Max Planck Society (MPS) and the Max Planck – EPFL Center for support. J.V.M. is grateful to the SNSF grant No. 193174. D.J.K acknowledges funding from the European Union's Horizon 2020 research and innovation programme under the Marie Skłodowska-Curie grant agreement No. 841136. The authors are grateful to Pierre Mettraux (EPFL) for his support in X-ray photoelectron spectroscopy, Rotraut Merkle (MPS) for support in TGA experiments, and Helga Hoier (MPS) for grazing incidence measurements. L.E. is grateful for financial support from SNSF Grant No. 200020_178860.

REFERENCES

(1) Jena, A. K.; Kulkarni, A.; Miyasaka, T. Halide Perovskite Photovoltaics: Background, Status, and Future Prospects. *Chem. Rev.* **2019**, *119*, 3036–3103. https://doi.org/10.1021/acs.chemrev.8b00539.

(2) Van Le, Q.; Jang, H. W.; Kim, S. Y. Recent Advances toward High-Efficiency Halide Perovskite Light-Emitting Diodes: Review and Perspective. *Small Methods* **2018**, *2*, 1700419. https://doi.org/10.1002/smtd.201700419.

(3) Senocrate, A.; Kim, G. Y.; Grätzel, M.; Maier, J. Thermochemical Stability of Hybrid Halide Perovskites. *ACS Energy Lett.* **2019**, *4*, 2859–2870. https://doi.org/10.1021/acsenergylett.9b01605.

(4) Kieslich, G.; Sun, S.; Cheetham, A. K. Solid-State Principles Applied to Organic–Inorganic Perovskites: New Tricks for an Old Dog. *Chem. Sci.* **2014**, *5*, 4712–4715. https://doi.org/10.1039/c4sc02211d.

(5) Saparov, B.; Mitzi, D. B. Organic − Inorganic Perovskites : Structural Versatility for Functional Materials Design. *Chem. Rev.* **2016**, *116*, 4558–4596. https://doi.org/10.1021/acs.chemrev.5b00715.

(6) Grancini, G.; Nazeeruddin, M. K. Dimensional Tailoring of Hybrid Perovskites for Photovoltaics. *Nat. Rev. Mater.* **2019**, *4*, 4–22. https://doi.org/10.1038/s41578-018-0065-0.

(7) Mao, L.; Stoumpos, C. C.; Kanatzidis, M. G. Two-Dimensional Hybrid Halide Perovskites: Principles and Promises. *J. Am. Chem. Soc.* **2018**, *141*, 1171–1190. https://doi.org/10.1021/jacs.8b10851.

(8) Chen, Y.; Sun, Y.; Peng, J.; Tang, J.; Zheng, K.; Liang, Z. 2D Ruddlesden – Popper Perovskites for Optoelectronics. *Adv. Mater.* **2017**, 1703487. https://doi.org/10.1002/adma.201703487.

(9) Stoumpos, C. C.; Cao, D. H.; Clark, D. J.; Young, J.; Rondinelli, J. M.; Jang, J. I.; Hupp, J. T.; Kanatzidis, M. G. Ruddlesden − Popper Hybrid Lead Iodide Perovskite 2D Homologous Semiconductors. *Chem. Mater.* **2016**, *28*, 2852–2867. https://doi.org/10.1021/acs.chemmater.6b00847.

(10) Mao, L.; Ke, W.; Pedesseau, L.; Wu, Y.; Katan, C.; Even, J.; Wasielewski, M. R.; Stoumpos, C. C.; Kanatzidis, M. G. Hybrid Dion–Jacobson 2D Lead Iodide Perovskites. *J. Am. Chem. Soc.* **2018**, *140*, 3775–3783. https://doi.org/10.1021/jacs.8b00542.

(11) Li, Y.; Milic, J. V; Ummadisingu, A.; Seo, J.; Im, J.; Kim, H.; Liu, Y.; Dar, M. I.; Zakeeruddin, S. M.; Wang, P.; Hagfeldt, A.; Graetzel, M. Bifunctional Organic Spacers for Formamidinium-Based Hybrid Dion−Jacobson Two-Dimensional Perovskite Solar Cells. *Nano Lett.* **2019**, *19*, 150–157. https://doi.org/10.1021/acs.nanolett.8b03552.

(12) Yan, J.; Fu, W.; Zhang, X.; Chen, J.; Yang, W.; Qiu, W.; Wang, M.; Liu, F.; Heremans, P.; Chen, H. Highly Oriented Two-Dimensional Formamidinium Lead Iodide Perovskite with a Small Bandgap of 1.51 eV. *Mater. Chem. Front.* **2018**, *2*, 121–128. https://doi.org/10.1039/C7QM00472A.

(13) Liu, Y.; Akin, S.; Pan, L.; Uchida, R.; Arora, N.; Milić, J. V; Hinderhofer, A.; Schreiber, F.; Uhl, A. R.; Zakeeruddin, S. M.; Hagfeldt, A.; Dar, M. I.; Grätzel, M. Ultrahydrophobic 3D/2D Fluoroarene Bilayer-Based Water-Resistant Perovskite Solar Cells with Efficiencies Exceeding 22%. *Sci. Adv.* **2019**, *5*, 1–9.

(14) Tsai, H.; Nie, W.; Blancon, J.; Stoumpos, C. C.; Asadpour, R.; Harutyunyan, B.; Neukirch, A. J.; Verduzco, R.; Crochet, J. J.; Tretiak, S.; Pedesseau, L.; Even, J.; Alam, M. A.; Gupta, G.; Lou, J.; Ajayan, P. M.; Bedzyk, M. J.; Kanatzidis, M. G.; Mohite, A. D. High-Efficiency Two-Dimensional Ruddlesden–Popper Perovskite Solar Cells. *Nature* **2016**, *536*, 312–316. https://doi.org/10.1038/nature18306.

(15) Smith, I. C.; Hoke, E. T.; Solis-Ibarra, D.; Mcgehee, M. D.; Karunadasa, H. I. A Layered Hybrid Perovskite Solar-Cell Absorber with Enhanced Moisture Stability. *Angew. Chem., Int. Ed.* **2014**, *53*, 11232–11235. https://doi.org/10.1002/anie.201406466.

(16) Schlipf, J.; Hu, Y.; Pratap, S.; Bießmann, L.; Hohn, N.; Porcar, L.; Bein, T.; Docampo, P.; Mu, P. Shedding Light on the Moisture Stability of 3D/2D Hybrid Perovskite Heterojunction Thin Films. ACS *Appl. Energy Mater.* **2019**, *2*, 1011–1018. https://doi.org/10.1021/acsaem.9b00005.

(17) Wygant, B. R.; Ye, A. Z.; Dolocan, A.; Vu, Q.; Abbot, D. M.; Mullins, C. B. Probing the Degradation Chemistry and Enhanced Stability of 2D Organolead Halide Perovskites. *J. Am. Chem. Soc.* **2019**, *141*, 18170–18181. https://doi.org/10.1021/jacs.9b08895.

(18) Wygant, B. R.; Geberth, G. T.; Ye, A. Z.; Dolocan, A.; Cotton, E.; Roberts, S. T.; Bout, D. A. Vanden; Mullins, C. B. Moisture-Driven Formation and Growth of Quasi-2D Organolead Halide Perovskite Crystallites. *ACS Appl. Energy Mater.* **2020**, *3*, 6280–6290. https://doi.org/10.1021/acsaem.0c00423.

(19) Soe Myae, C. M.; Nagabhushana, G. P.; Shivaramaiah, R.; Tsai, H.; Nie, W.; Blancon, J.; Cao, D. H.; Traoré, B.; Pedesseau, L.; Kepenekian, M.; Katan, C.; Even, J.; J. Marks, T.; Navrotsky, A.; Mohite, A. D.; Stoumpos, C. C.; Kanatzidis, M. G. Structural and Thermodynamic Limits of Layer Thickness in 2D Halide Perovskites. *PNAS* **2019**, *116*, 58–66. https://doi.org/10.1073/pnas.1811006115.

(20) Ahmad, S.; Fu, P.; Yu, S.; Yang, Q.; Liu, X.; Wang, X.; Wang, X.; Guo, X.; Li, C. Dion–Jacobson Phase 2D Layered Perovskites for Solar Cells with Ultrahigh Stability. *Joule* **2019**, *3*, 1–13. https://doi.org/10.1016/j.joule.2018.11.026.

(21) Li, X.; Ke, W.; Traoré, B.; Guo, P.; Hadar, I.; Kepenekian, M.; Even, J.; Katan, C.; Stoumpos, C. C.; Schaller, R. D.; Kanatzidis, M. G. Two-Dimensional Dion–Jacobson Hybrid Lead Iodide Perovskites with Aromatic Diammonium Cations. *J. Am. Chem. Soc.* **2019**, *141*, 12880–12890. https://doi.org/10.1021/jacs.9b06398.

(22) Xu, Z.; Chen, M.; Liu, S. F. First-Principles Study of Enhanced Out-of-Plane Transport Properties and Stability in Dion–Jacobson Two-Dimensional Perovskite Semiconductors for High-Performance Solar Cell Applications. *J. Phys. Chem. Lett.* **2019**, *10*, 3670–3675. https://doi.org/10.1021/acs.jpclett.9b01360.

(23) Huang, P.; Kazim, S.; Wang, M.; Ahmad, S. Toward Phase Stability: Dion–Jacobson Layered Perovskite for Solar Cells. *ACS Energy Lett.* **2019**, *4*, 2960–2974. https://doi.org/10.1021/acsenergylett.9b02063.

(24) Lermer, C.; Senocrate, A.; Moudrakovski, I.; Seewald, T.; Hatz, A. K.; Mayer, P.; Pielnhofer, F.; Jaser, J. A.; Schmidt-Mende, L.; Maier, J.; Lotsch, B. V. Completing the Picture of 2-(Aminomethylpyridinium) Lead Hybrid Perovskites: Insights into Structure, Conductivity Behavior, and Optical Properties. *Chem. Mater.* **2018**, *30*, 6289–6297. https://doi.org/10.1021/acs.chemmater.8b01840.

(25) Lemmerer, A.; Billing, D. G. Two Packing Motifs Based upon Chains of Edge-Sharing PbI_6 Octahedra. *Acta Crystallogr. Sect. C Cryst. Struct. Commun.* **2006**, *62*, 597–601. https://doi.org/10.1107/S0108270106039746.

(26) Cohen, B.; Li, Y.; Meng, Q.; Etgar, L. Dion–Jacobson Two-Dimensional Perovskite Solar Cells Based on Benzene Dimethanammonium Cation. *Nano Lett.* **2019**, *19*, 2588–2597. https://doi.org/10.1021/acs.nanolett.9b00387.

(27) Hou, M.; Xu, Y.; Zhou, B.; Tian, Y.; Wu, Y.; Zhang, D.; Wang, G.; Li, B.; Ren, H.; Li, Y.; Huang, Q.; Ding, Y.; Zhao, Y.; Zhang, X.; Hou, G. Aryl Diammonium Iodide Passivation for Efficient and Stable Hybrid Organ-Inorganic Perovskite Solar Cells. *Adv. Funct. Mater.* **2020**, 2002366. https://doi.org/10.1002/adfm.202002366.

(28) Gélvez-Rueda, M. C.; Ahlawat, P.; Merten, L.; Jahanbakhshi, F.; Mladenović, M.; Hinderhofer, A.; Dar, M. I.; Li, Y.; Dučinskas, A.; Carlsen, B.; Tress, W.; Ummadisingu, A.; Zakeeruddin, S. M.; Schreiber, F.; Hagfeldt, A.; Rothlisberger, U.; Grozema, F. C.; Milić, J. V.; Graetzel, M. Formamidinium-Based Dion–

Jacobson Layered Hybrid Perovskites: Structural Complexity and Optoelectronic Properties. *Adv. Funct. Mater.* **2020**, *30*, 2003428. https://doi.org/10.1002/adfm.202003428.

(29) Mao, L.; Tsai, H.; Nie, W.; Ma, L.; Im, J.; Stoumpos, C. C.; Malliakas, C. D.; Hao, F.; Wasielewski, M. R.; Mohite, A. D.; Kanatzidis, M. G. Role of Organic Counterion in Lead- and Tin-Based Two-Dimensional Semiconducting Iodide Perovskites and Application in Planar Solar Cells. *Chem. Mater.* **2016**, *28*, 7781–7792. https://doi.org/10.1021/acs.chemmater.6b03054.

(30) Kagan, C. R.; Mitzi, D. B.; Dimitrakopoulos, C. D. Organic-Inorganic Hybrid Materials as Semiconducting Channels in Thin-Film Field-Effect Transistors. *Science* **1999**, *286*, 945–948.

(31) Chen, A. Z.; Shiu, M.; Ma, J. H.; Alpert, M. R.; Zhang, D.; Foley, B. J.; Smilgies, D.; Lee, S.; Choi, J. J. Origin of Vertical Orientation in Two-Dimensional Metal Halide Perovskites and Its Effect on Photovoltaic Performance. *Nat. Commun.* **2018**, *9*, 1336. https://doi.org/10.1038/s41467-018-03757-0.

(32) Yu, S.; Yan, Y.; Abdellah, M.; Pullerits, T.; Zheng, K.; Liang, Z. Nonconfinement Structure Revealed in Dion – Jacobson Type Quasi-2D Perovskite Expedites Interlayer Charge Transport. *Small* **2019**, *15*, 1905081. https://doi.org/10.1002/smll.201905081.

(33) Bondi, A. Van Der Waals Volumes and Radii. *J. Phys. Chem.* **1964**, *68*, 441–451. https://doi.org/10.1021/j100785a001.

(34) Blancon, J.; Stier, A. V; Tsai, H.; Nie, W.; Stoumpos, C. C.; Traoré, B.; Pedesseau, L.; Kepenekian, M.; Katsutani, F.; Noe, G. T.; Kono, J.; Tretiak, S.; Crooker, S. A.; Katan, C.; Kanatzidis, M. G.; Crochet, J. J.; Even, J.; Mohite, A. D. Scaling Law for Excitons in 2D Perovskite Quantum Wells. *Nat. Commun.* **2018**, *9*, 2254. https://doi.org/10.1038/s41467-018-04659-x.

(35) Ishihara, T. Optical Properties of PbI-Based Perovskite Structures. *J. Lumin.* **1994**, *60–61*, 269–274. https://doi.org/10.1016/0022-2313(94)90145-7.

(36) Cao, X. B.; Li, C. L.; Zhi, L. L.; Li, Y. H.; Cui, X.; Yao, Y. W.; Ci, L. J.; Wei, J. Q. Fabrication of High Quality Perovskite Films by Modulating the Pb-O Bonds in Lewis Acid-Base Adducts. *J. Mater. Chem. A* **2017**, *5*, 8416–8422. https://doi.org/10.1039/c7ta00539c.

(37) Frisch, M. J.; Trucks, G. W.; Schlegel, H. B.; Scuseria, G. E.; Robb, M. A.; Cheeseman, J. R.; Scalmani, G.; Barone, V.; Mennucci, B.; Petersson, G. A.; Nakatsuji, H.; Caricato, M.; Li, X.; Hratchian, H. P.; Izmaylov, A. F.; Bloino, J.; Zheng, G.; Sonnenb, D. J. Gaussian 09, Revision A.1. Gaussian Inc. Wallingford CT 2009 2009.

(38) Leguy, M. A.; Hu, Y.; Campoy-quiles, M.; Alonso, M. I.; Weber, O. J.; Azarhoosh, P.; Schilfgaarde, M. Van; Weller, M. T.; Bein, T.; Nelson, J.; Docampo, P.; Barnes, P. R. F. Reversible Hydration of

$CH_3NH_3PbI_3$ in Films, Single Crystals, and Solar Cells. *Chem. Mater.* **2015**, *27*, 3397–3407. https://doi.org/10.1021/acs.chemmater.5b00660.

(39) Imler, G. H.; Li, X.; Xu, B.; Dobereiner, G. E.; Dai, H.; Rao, Y.; Wayland, B. B. Solid State Transformation of the Crystalline Monohydrate $(CH_3NH_3)PbI_3(H_2O)$ to the $(CH_3NH_3)PbI_3$ Perovskite. *ChemComm* **2015**, *51*, 11290–11292. https://doi.org/10.1039/c5cc03741g.

(40) Wang, G. E.; Wang, M. S.; Jiang, X. M.; Liu, Z. F.; Lin, R. G.; Cai, L. Z.; Guo, G. C.; Huang, J. S. Crystal Structures and Optical Properties of 1-D Iodoplumbates Templated by in Situ Synthesized p-Phenylenediamine Derivatives. *Inorg. Chem. Commun.* **2011**, *14*, 1957–1961. https://doi.org/10.1016/j.inoche.2011.09.020.

(41) Kamminga, M. E.; De Wijs, G. A.; Havenith, R. W. A.; Blake, G. R.; Palstra, T. T. M. The Role of Connectivity on Electronic Properties of Lead Iodide Perovskite-Derived Compounds. *Inorg. Chem.* **2017**, *56*, 8408–8414. https://doi.org/10.1021/acs.inorgchem.7b01096.

(42) Safdari, M.; Svensson, P. H.; Hoang, M. T.; Oh, I.; Kloo, L.; Gardner, J. M. Layered 2D Alkyldiammonium Lead Iodide Perovskites: Synthesis, Characterization, and Use in Solar Cells. *J. Mater. Chem. A* **2016**, *4*, 15638–15646. https://doi.org/10.1039/c6ta05055g.

(43) Wang, F.; Geng, W.; Zhou, Y.; Fang, H. H.; Tong, C. J.; Loi, M. A.; Liu, L. M.; Zhao, N. Phenylalkylamine Passivation of Organolead Halide Perovskites Enabling High-Efficiency and Air-Stable Photovoltaic Cells. *Adv. Mater.* **2016**, *28*, 9986–9992. https://doi.org/10.1002/adma.201603062.

(44) Ma, C.; Shen, D.; Huang, B.; Li, X.; Chen, W. C.; Lo, M. F.; Wang, P.; Hon-Wah Lam, M.; Lu, Y.; Ma, B.; Lee, C. S. High Performance Low-Dimensional Perovskite Solar Cells Based on a One Dimensional Lead Iodide Perovskite. *J. Mater. Chem. A* **2019**, *7*, 8811–8817. https://doi.org/10.1039/c9ta01859j.

(45) Lin, J.; Lai, M.; Dou, L.; Kley, C. S.; Chen, H.; Peng, F.; Sun, J.; Lu, D.; Hawks, S. A.; Xie, C.; Cui, F.; Alivisatos, A. P.; Limmer, D. T.; Yang, P. Thermochromic Halide Perovskite Solar Cells. *Nat. Mater.* **2018**, *17*, 261–267. https://doi.org/10.1038/s41563-017-0006-0.

(46) Yang, J.; Siempelkamp, B. D.; Liu, D.; Kelly, T. L. Investigation of $CH_3NH_3PbI_3$ Degradation Rates and Mechanisms in Controlled Humidity Environments Using in Situ Techniques. *ACS Nano* **2015**, *9*, 1955–1963. https://doi.org/10.1021/nn506864k.

(47) Ouyang, Y.; Li, Y.; Zhu, P.; Li, Q.; Gao, Y.; Tong, J.; Shi, L.; Zhou, Q.; Ling, C.; Chen, Q.; Deng, Z.; Tan, H.; Deng, W.; Wang, J. Photo-Oxidative Degradation of Methylammonium Lead Iodide Perovskite: Mechanism and Protection. *J. Mater. Chem. A* **2019**, *7*, 2275–2282. https://doi.org/10.1039/c8ta12193a.